Indoor Air Quality Implications of Germicidal 222 nm Light

Indoor Air Quality Implications of Germicidal 222 nm Light

Victoria Barber[1,2$*], Matthew B. Goss[1$], Lesly J. Franco Deloya[4], Lexy N. LeMar[5], Yaowei Li[6], Erik Helstrom[1], Manjula Canagaratna[7], Frank N. Keutsch[6,8,9], Jesse H. Kroll[1,5*]

[1]Department of Civil and Environmental Engineering, Massachusetts Institute of Technology, Cambridge, Massachusetts 02139, United States
[2]now at Department of Chemistry and Biochemistry, University of California Los Angeles, Los Angeles, California, 90095
[4]Department of Earth, Atmospheric, and Planetary Sciences, Massachusetts Institute of Technology, Cambridge, Massachusetts 02139, United States
[5]Department of Chemical Engineering, Massachusetts Institute of Technology, Cambridge, Massachusetts 02139, United States
[6]John A. Paulson School of Engineering and Applied Sciences, Harvard University, Cambridge, Massachusetts 02138, United States
[7]Center for Aerosol and Cloud Chemistry, Aerodyne Research Incorporated, Billerica, Massachusetts 01821, United States
[8]Department of Chemistry and Chemical Biology, Harvard University, Cambridge, Massachusetts 02138, United States
[9]Department of Earth and Planetary Sciences, Harvard University, Cambridge, Massachusetts 02138, United States
[$]V.P.B. and M.B.G. contributed equally to this work [*]Corresponding Authors

Email: vbarber@chem.ucla.edu
Phone: 424-259-5198
University of California, Los Angeles
Department of Chemistry and Biochemistry
607 Charles E. Young Drive, East, YH3077B
Los Angeles, CA 90095

Email: jhkroll@mit.edu
Phone: 617-253-2409
Massachusetts Institute of Technology
Department of Civil and Environmental Engineering
77 Massachusetts Avenue, 48-331
Cambridge, MA 02139

Keywords: Ultraviolet Germicidal Irradiation, Indoor Air Quality, Ozone, Photochemistry, Ventilation, Volatile Organic Compounds, Secondary Organic Aerosol

Abstract

One strategy for mitigating the indoor transmission of airborne pathogens, including the SARS-CoV-2 virus, is irradiation by germicidal UV light (GUV). A particularly promising approach is 222 nm light from KrCl excimer lamps (GUV_{222}); this inactivates airborne pathogens and is thought to be relatively safe for human skin and eye exposure. However, the impact of GUV_{222} on the composition of indoor air has received little experimental study. Here, we conduct laboratory experiments in a 150 L Teflon chamber to examine the formation of secondary species by GUV_{222}. We show that GUV_{222} generates ozone (O_3) and hydroxyl radicals (OH), both of which can react with volatile organic compounds to form oxidized volatile organic compounds and secondary organic aerosol particles. Results are consistent with a box model based on known photochemistry. We use this model to simulate GUV_{222} irradiation under more realistic indoor air scenarios, and demonstrate that under some conditions, GUV_{222} irradiation can lead to levels of O_3, OH, and secondary organic products that are substantially elevated relative to normal indoor conditions. The results suggest that GUV_{222} should be used at low intensities and in concert with ventilation, decreasing levels of airborne pathogens while mitigating the formation of air pollutants.

Synopsis

Germicidal ultraviolet light at 222 nm (GUV_{222}) can inactivate airborne pathogens, but has an unknown effect on indoor air quality. This study shows that GUV_{222} forms ozone and hydroxyl radicals, forming oxidized byproducts and fine particulate matter.

TOC Graphic

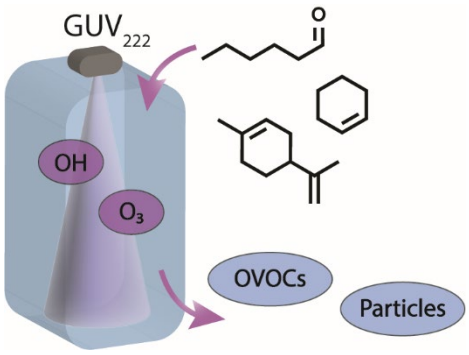

Introduction

The COVID-19 pandemic has highlighted the critical need to develop and implement strategies to decrease the transmission of airborne pathogens. Approaches include both source control (isolation, masking), and remediation (ventilation, air cleaning). One approach that has received substantial attention is the use of germicidal ultraviolet (GUV) light, which inactivates airborne pathogens. This approach goes back decades,[1] traditionally using 254 nm light from mercury lamps. Since light of this wavelength can cause damage to skin and eyes, care must be taken to minimize occupants' direct exposure to the GUV light.[2,3]

A promising new approach to GUV-based air cleaning is the use of KrCl excimer lamps, which emit at 222 nm (GUV_{222}).[4] In contrast to 254 nm GUV, GUV_{222} does not penetrate deeply into biological materials. Therefore, while GUV_{222} is effective at inactivating airborne viruses and bacteria, it is unable to penetrate the outer layer of dead skin cells or the ocular tear layer.[5] 222 nm light is hence less likely to reach and damage living human tissues, offering the potential for air disinfection throughout an entire, occupied indoor space.

A risk with GUV_{222}-based air cleaning, as with all types of air cleaning that rely on chemical and/or photolytic processes, is the potential formation of unwanted secondary byproducts.[6,7] A particular concern with GUV_{222} is the formation of ozone (O_3), a harmful air pollutant that acts as a strong oxidant and can lead to respiratory distress when inhaled.[8] O_3 is formed by the UV photodissociation of oxygen (R1-2)

$$O_2 + h\nu_{\lambda<242\ nm} \rightarrow O + O \quad \text{(R1)}$$

$$O + O_2 + M \rightarrow O_3 + M \quad \text{(R2)}$$

Since absorption of UV by O_2, and hence O_3 production, is strongest at short wavelengths,[9] manufacturers of KrCl lamps have added filters to block wavelengths shorter than 222 nm. But since O_2 absorbs weakly even at 222 nm ($\sigma = 4.09 \times 10^{-24}$ cm^2 [9]), all KrCl lamps have the potential to generate ozone, possibly in concentrations higher than is typically found indoors.[10]

Ozone generated indoors, in addition to posing a direct health hazard, can set off a cascade of chemical reactions that can also affect indoor air quality. Ozone reacts directly with alkenes, present both in the air and on indoor surfaces, forming a range of oxidized volatile organic compounds (OVOCs)[11,12] and secondary organic aerosol (SOA),[13] which may negatively impact human health.[14–17] O_3 chemistry can also lead to the formation of the hydroxyl radical (OH), an even stronger oxidant. This occurs both through reactions with alkenes, which are known to form OH (R3),[11,18] and through O_3 photolysis (R4-5)[19]:

$$\text{Alkene} + O_3 \rightarrow \text{OH} + \text{other products} \quad \text{(R3)}$$

$$O_3 + h\nu_{\lambda<\sim370\ nm} \rightarrow O_2 + O(^1D) \quad \text{(R4)}$$

$$O(^1D) + H_2O \rightarrow 2OH \quad \text{(R5)}$$

Any increased levels of indoor O_3 from GUV_{222} would likely enhance the importance of these reactions, leading to higher levels of indoor OH. This includes O_3 photolysis (R4-5), which is the

main source of OH in the troposphere, but under normal conditions is negligible in indoor environments, due to the lack of low-wavelength UV. Any OH radicals formed from R3-5 may then oxidize a wide range of organic species and contribute further to the formation of OVOCs and SOA.

GUV_{222} therefore has the potential to dramatically affect the chemical composition of indoor air, and may lead to the formation of chemical species that are hazardous to human health. However, the extent and nature of this impact remains quite uncertain, even as GUV_{222} is being deployed in indoor spaces.[20] Two very recent experimental studies[21,22] demonstrate O_3 production from GUV_{222}, but these do not examine the overall effects on indoor air quality (including the production of OH, OVOCs, and SOA) by GUV_{222}. To our knowledge the only published work that has is a box-modeling study by Peng et al.[23]. That work predicted that 222 nm irradiation could lead to elevated levels of O_3 and other secondary species relative to non-illuminated conditions, especially under low-ventilation conditions.

Here we describe a series of laboratory experiments aimed at better understanding the effects of 222 nm irradiation on indoor air quality. The goal of this work is to gain process-based insight into how such irradiation affects the chemical composition of the air; we do not examine the effects of GUV_{222} light on pathogens, indoor surfaces, or human health. These experiments, which use a flow-through Teflon chamber coupled to a range of real-time analytical instruments, explore the effects of several parameters relevant to indoor air processes (VOC level, ventilation, 222 nm light intensity, and humidity) on the generation of oxidants and secondary products. Results are then used to validate a simple chemical model of GUV_{222} irradiation of indoor air, which in turn is used to examine the interplay between GUV_{222} and ventilation in controlling the levels of ozone and other chemical species in the indoor environment.

Materials and Methods

Experimental Methods

Experiments are carried out in a 150 L Teflon chamber, outfitted with inlet ports (for introduction of clean air and trace species) and outlet ports (for sampling by analytical instrumentation). Clean dry air from a zero-air generator (Aadco Model 737) is introduced into the chamber either directly, or after passing through a bubbler filled with Milli-Q water. Mass flow controllers are used to adjust these two flows to control chamber relative humidity. Dilution rates are measured using acetonitrile, an inert dilution tracer (8.0×10^{-4} – 9.7×10^{-4} s^{-1}, 2.9 – 3.5 ACH). Most experiments are conducted at 22°C and ~25% RH, while "higher RH" experiments are carried out at ~45% RH.

GUV_{222} light is provided by a single filtered KrCl excimer lamp (Ushio, Care222 B1 Illuminator, peak emission at 222 nm), centered directly above the Teflon chamber. Average fluence rate within the chamber is ~45 $\mu W/cm^2$, estimated geometrically from the lamp intensity profile provided by the manufacturer[24] (see Section S1.1). The indirect estimation of the lamp intensity is a limitation of this work, but the agreement between modeled and measured ozone production (see Results and Discussion, below) indicates that it is reasonably accurate. More quantitative estimates of UV fluence rate and its relationship to O_3 generation are available in recent work by

Peng et al.[22] and Link et al.[21] Most experiments are carried out at the full light intensity. For "low light" experiments, the lamp emission is attenuated by several layerPs of plastic, achieving a factor of ~5 reduction in intensity (determined by the reduction in the steady-state O_3 concentration which is assumed to scale linearly with average UV fluence).[21,22] For the "O_3-only" experiments, the light is left off, and O_3 is introduced via a Pen-Ray ozone generator, with a steady-state O_3 concentration matching that of the GUV_{222} experiments (~100 ppb). Reaction conditions for each experiment are described in detail in Table S1.

For all VOC oxidation experiments, the chamber is first allowed to reach a steady-state concentration of O_3, either via 222 nm irradiation or direct addition. This is followed by the addition of 5.3 ppb of acetonitrile (the dilution tracer) (C_2H_3N, 99.8%, Sigma Aldrich), 1.2 ppb of 1-butan-d9-ol (intended as an OH tracer, but not used here due to the relatively low OH levels) (C_4D_9OH, 98%, Cambridge Isotope Laboratories, Inc.), and 120 ± 11 μg m^{-3} of ammonium sulfate particles (to act as seed particles for any SOA production) ($(NH_4)_2SO_4$, ≥99%, Sigma Aldrich). Finally, the relevant VOC (10 or 100 ppb) is added to chamber. VOCs used in this study include hexanal ($C_6H_{12}O$, 98%, Sigma Aldrich), cyclohexene (C_6H_{10}, 99%, Sigma Aldrich), and (R)-(+)-limonene ($C_{10}H_{16}$, 97%, Sigma Aldrich). Reactant addition procedures are described in greater detail in Section S1.2. Because the oxidants are already present in the chamber, oxidation begins immediately, so VOC injection is taken as t = 0.

Real-time measurements of gas- and particle-phase composition in the chamber are conducted using a suite of analytical instruments. Ozone is measured by a UV absorption monitor (2BTech). NO_x is monitored using a chemiluminescence NO-NO_2-NO_X analyzer (Thermo Fisher Scientific) and was below the instrument detection limit in all experiments. Reactant VOC and OVOC products are monitored using a Vocus proton transfer-reaction mass spectrometer (PTR-MS, Tofwerk, Aerodyne Research, Inc.[25]), and an ammonium chemical ionization mass spectrometer (NH_4^+ CIMS, modified PTR3, see Zaytsev et al.[26]). Particle concentration and composition are measured using a scanning mobility particle sizer (SMPS, TSI) and an aerosol mass spectrometer (AMS, Aerodyne Research, Inc.[27]). Analytical instruments are summarized in Table S2. Gas-phase mass spectrometric data is background-subtracted and corrected for dilution. The analysis does not account for variations in detection efficiencies, which may be substantial,[26] and we therefore report relative signals, which are unaffected by such calibration uncertainties, rather than absolute concentrations. Particle-phase data is corrected for dilution and wall losses by normalizing to the ammonium sulfate seed particle concentration. Data analysis and quantification approaches are described in more detail in Section S1.3.

Results and Discussion

Ozone production

The production of ozone by 222 nm light is examined via the irradiation of clean chamber air. Figure 1 shows results from four representative irradiation experiments, run at different ventilation rates (1.3 to 3.1 air changes per hour (ACH)) and relative humidities (25%-45%). O_3 production is observed to occur immediately when the lights are turned on. O_3 levels increase quickly at first, eventually leveling off to a steady-state value, in which photolytic production is balanced by removal by outflow. The O_3 production rate is measured at 324 ± 18 ppb hr^{-1}, in reasonably good agreement with previous measurements[22] when differences in average GUV_{222}

fluence rate are considered (see Section S3.1). The steady-state O_3 concentration is independent of relative humidity, and inversely proportional to ventilation rate (Figure S3).

Dashed lines in Figure 1 denote O_3 concentrations predicted from a simple box model. This model includes O_2 photolysis (R1-2), O_x-HO_x chemistry, and dilution (See Table S3 for rate constants and photochemical parameters[9–11,28–32]). Model parameters (e.g., light intensity, air-exchange rate, and RH) are matched to each experiment. O_3 deposition, which is likely small on Teflon surfaces, is not included. The model accurately predicts measured O_3 levels, indicating that the processes describing ozone levels (formation from O_3 photolysis at 222 nm, loss by outflow) are well-captured by the simple model.

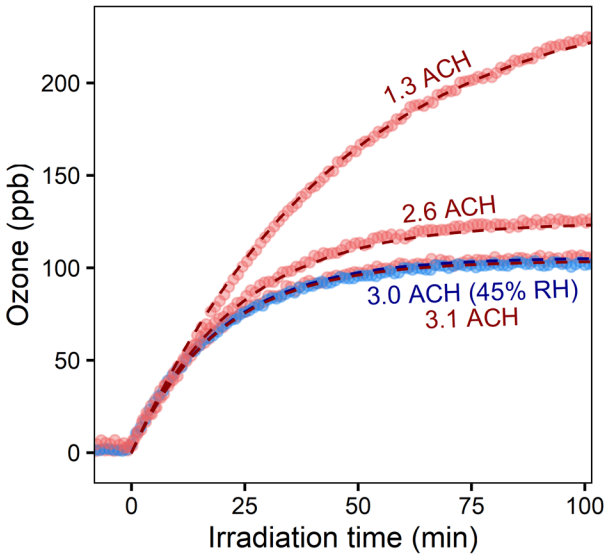

Figure 1: Observed ozone production for clean-chamber irradiation experiments. Measurements agree well with the predictions from the simple box model (dashed lines) across a range of ventilation rates and relative humidities. Measurements shown in red are taken at 25% RH.

Decay of VOCs upon 222 nm irradiation.

In a second set of experiments (Table S1), VOCs are added to the irradiated chamber after O_3 levels reach steady state. Experiments center on two VOCs: hexanal, a C6 compound that reacts only with OH, and cyclohexene, a C6 compound that reacts with both OH and O_3. VOC decays are shown in Figure 2. Negligible change in O_3 concentration is observed upon introduction of 10 ppb of VOC; when 100 ppb of cyclohexene is introduced, a small O_3 depletion (~4.3 ppb) is observed.

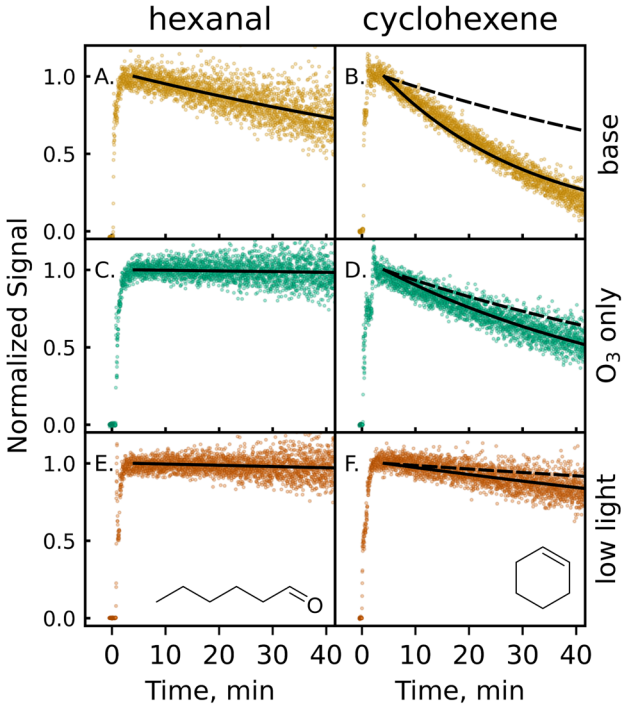

Figure 2: Normalized decays of two VOCs (hexanal and cyclohexene) after introduction to the GUV_{222}-irradiated chamber (see also Figure S4). Time = 0 refers to when the VOC was injected into the chamber. Traces are background- and dilution-corrected, so observed decays are from oxidative loss only. Details of each experimental condition (base, O_3 only, low light) are given in the text and Table S1. Solid black lines denote single-exponential fits to the observed decays; dashed black lines show the expected decay of cyclohexene from reaction with O_3 only.[28]

Under "base conditions" (10 ppb VOC precursor, 222 nm light, ~25% RH) (Figure 2AB), the concentrations of both hexanal and cyclohexene decrease after being introduced to the irradiated chamber. Concentrations are corrected for dilution; losses by direct photolysis and uptake to surfaces are expected to be minimal (see Section S3.2). Therefore, decays indicate oxidative loss only. This oxidation cannot be explained by O_3 alone. Hexanal does not react with O_3 – a very small decay of hexanal is attributed to minor, non-oxidative loss pathways (see SI). While cyclohexene does react with O_3, its decay is far faster than what can be attributed to the O_3 reaction (dashed line). Indeed, for experiments in which the GUV_{222} light is off and VOCs are exposed to the same levels of O_3 as in the irradiated case (Figure 2CD), the hexanal does not decrease at all, and cyclohexene decays far less than in the irradiation case, at a rate consistent with reaction with O_3 (plus a small contribution from OH generated by the ozonolysis reaction, reaction R3). This observed "excess reactivity" (the difference in observed decays and decays expected from O_3 reaction alone) indicates that GUV_{222} irradiation generates not only O_3 but other oxidants as well.

Additional experiments carried out under a range of reaction conditions provide evidence that these additional oxidants are OH radicals, formed from reactions 3-5. For example, experiments with the 222 nm fluence rate attenuated substantially (~ 9 μW cm^{-2}, Figure 2EF) exhibit VOC decay rates that are much slower compared to those under base conditions. This attenuation is assumed to decrease steady-state O_3 concentrations proportionally. However, the observed excess reactivity disproportionately decreases, by approximately an order of magnitude. This is consistent with OH formation, which depends on the photolysis of both O_2 and O_3, as well as (in the case of cyclohexene) the ozonolysis reactions. The dependence of decays on other experimental parameters, such as VOC concentration and relative humidity, are also consistent with OH production from GUV_{222} lights; this is discussed in detail in Section S3.3.

We estimate average OH levels in all experiments using an exponential fit to the VOC timeseries and known OH rate constants.[29,30] For cyclohexene experiments, average measured [O_3] and the O_3 + cyclohexene rate constant are included in the fit to account for excess reactivity. The range of [OH] measured in each experiment is calculated by applying the same exponential fits to a rolling 15-minute window (see Section S3.4 for more details). We also calculate OH levels using our simple box model by including a highly simplified oxidation scheme (Table S3) for each injected VOC. Reaction rates of the VOC with OH and O_3 are taken from the literature, and oxidation products are assumed to have the same OH reactivities as their precursors. Measured and modeled average [OH] agree well (Figure 3), providing strong evidence that GUV_{222} produces not only O_3 (R1-2) but also OH (R3-5), and that oxidation by both O_3 and OH can take place upon irradiation with 222 nm light.

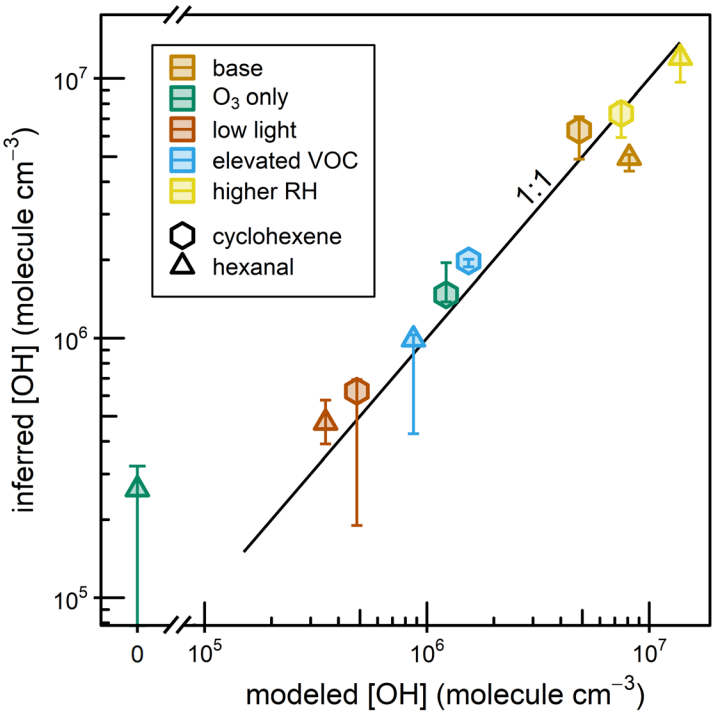

Figure 3: Experimentally-derived average OH concentration vs. average OH concentration predicted by the box model, for all cyclohexene and hexanal experiments (see Section S3.4).

Note the break in the x-axis. Error bars represent the range of values observed throughout the experiment.

Formation of gas-phase oxidation products

The formation of oxidized gas-phase products is observed in all experiments in which VOC oxidation occurs. Product distributions for three cyclohexene experiments (base conditions, O_3 only, and low light) are shown in Figure 4. Additional product distributions and time-series results (including for the hexanal experiments) are provided in Figures S5 and S6.

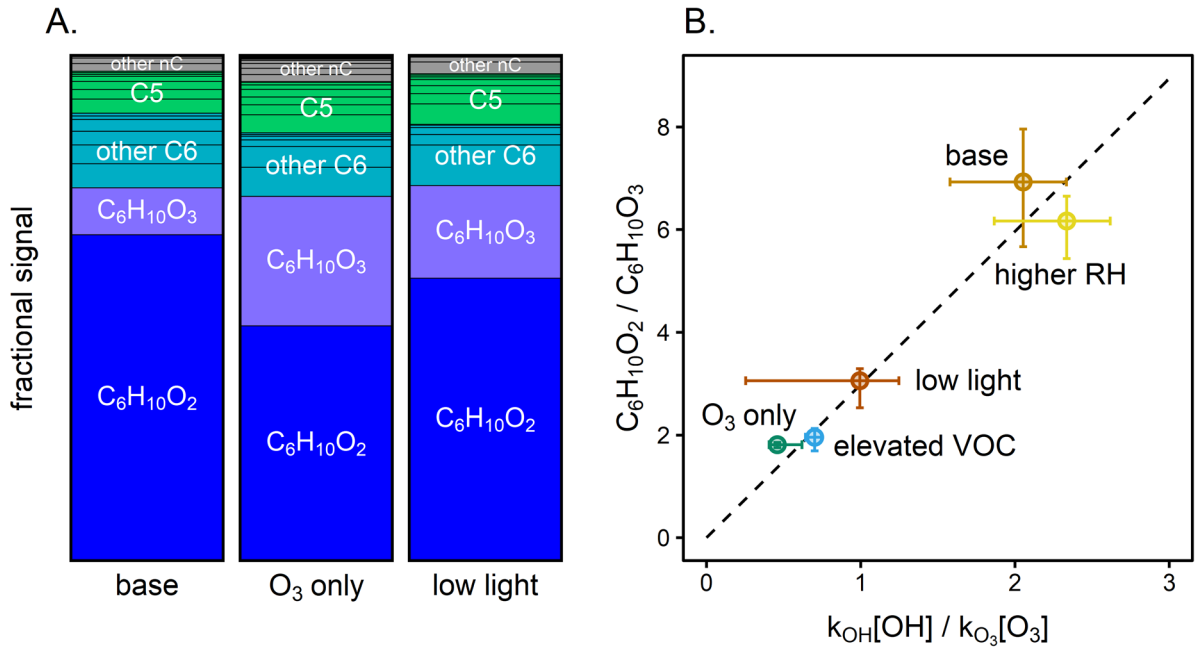

Figure 4: Gas-phase products from cyclohexene experiments. Panel A: Normalized mass spectrometric signal of products formed for the GUV_{222} irradiation (base conditions), O_3-only, and low-light experiments (see Section S3.5 for calculations and Figure S5 for other experimental conditions). Signals are integrated from t = 250 s to 2500 s, normalized to total integrated ion signal and grouped by carbon number (nC). In all cases products are dominated by $C_6H_{10}O_2$ (the major cyclohexene + OH reaction product) and $C_6H_{10}O_3$, (the major cyclohexene + O_3 product). Panel B: The ratio of the $C_6H_{10}O_2$-to-$C_6H_{10}O_3$ signals vs. the ratio of the rates of OH and O_3 oxidation, for all cyclohexene experiments. Concentrations of OH are determined from the fits in Figure 2, while concentrations of O_3 are measured directly. The dashed line is a linear fit to the data; since the two products have differing sensitivities in the instrument, this differs from the 1:1 line. Error bars represent the range of values observed throughout the experiment.

Measured products are dominated by C6 and C5 compounds, as expected given that cyclohexene is a C6 species. The two products with the largest mass spectrometric signals, $C_6H_{10}O_2$ and $C_6H_{10}O_3$, are the major products of the OH and O_3 initiated oxidation of cyclohexene, respectively[33,34] (see Scheme S1) (Products are detected as the analyte-NH_4^+ adduct, and reported

as the analyte formula.) The ratios of the signals from the two products vary among experiments, indicating differences in the relative concentrations of OH and O_3. In Figure 4b, the ratio of the mass spectrometric signals of these two products is shown vs. the relative OH-to-O_3 oxidation rate ratios (calculated from the experimentally-determined values of [OH] and [O_3]) for each cyclohexene experiment. A strong correlation ($R^2 = 0.98$) is found between the two ratios, providing further support for OH-initiated oxidation, and more generally for OH radical production from irradiation by 222 nm light. The products formed in the 222 nm irradiation of hexanal are also broadly consistent with OH-initiated oxidation (see Scheme S2).[35]

Secondary organic aerosol formation

In all experiments, dry ammonium sulfate seed particles are added to the chamber, providing surface area onto which low-volatility species may condense, and enabling the assessment of potential SOA formation. SOA formation is observed in a number of experiments (Table S1 and Figure S7). SOA formation is generally modest for most hexanal and cyclohexene experiments, likely due to the relatively small size (C6) and low concentrations (10 ppb) of those species. Higher concentrations of SOA are observed for experiments with high initial concentrations (100 ppb) of hexanal or cyclohexane, and for those using limonene ($C_{10}H_{16}$, a monoterpene commonly found in fragrances and cleaning products). In fact, the GUV_{222} irradiation of 100 ppb limonene (a level that can be found in indoor environments immediately after cleaning events[36,37]) results in exceedingly high SOA loadings, on the order of 400 ± 80 μg m^{-3}. Additionally, the formation of new particles is observed upon 222 nm irradiation under some conditions (Section S3.6 and Figure S8). This effect is not observed when O_3 is added without 222 nm irradiation. GUV_{222}-induced nucleation occurs even when no VOCs are added, and so may result from photochemistry of organic species on the chamber surfaces, or even of the surface materials themselves. Whether this is a general feature of the irradiation of organics on indoor surfaces is unclear from the present experiments, but it does suggest that 222 nm irradiation may induce new particle formation in some environments.

Extrapolation to indoor environments

The above laboratory experiments demonstrate that GUV_{222} irradiation forms ozone, OH, and a range of oxidation products; measured ozone and inferred OH agree broadly with predictions by a photochemical box model. However, real-world indoor environments are substantially different than our simple laboratory system: they involve a large number of organic compounds, depositional loss of ozone and other species, infiltration of outdoor pollutants, a wide range of possible ventilation rates, and typically much lower average UV fluence rates. Here we extend our photochemical model to a more realistic indoor air scenario, with the goal of understanding how GUV_{222} may impact indoor air quality under a range of ventilation and irradiation conditions.

For simulations of chemistry in a more realistic indoor environment, two "lumped" VOCs are included in the model: one (VOC1) that reacts with OH but not with O_3, and another (VOC2) that reacts with both OH and O_3. Rate constants for VOC1 are chosen based on typical values for indoor VOCs (Section S2.1 and Tables S3 and S4); rate constants for VOC2 are assumed to be equal to those of limonene. OH yields from O_3 + VOC2 are assumed to by 0.86, equal to that of limonene.[11] All oxidation reactions form lumped organic products that can also react with OH. VOC emission rates (84 ppb hr^{-1} and 4.2 ppb hr^{-1} for VOC1 and VOC2, respectively) are determined from previous measurements of OH and O_3 reactivities in indoor environments;[38,39] details of these calculations are given in Section S2.1. The model is run at 298 K, 1 atm, and 30% RH. We also include a background concentration of O_3 in the ventilation air (40 ppb, consistent with typical outdoor O_3 concentrations), a 25% loss of O_3 to the ventilation system, and an O_3 deposition constant of 3 hr^{-1} [10,31].

The range of light fluence rates chosen covers US and international guidelines on 222 nm exposure limits (ranging from 0.8 to 16 $\mu W/cm^2$ assuming a continuous 8-hour exposure[40,41]) as well as the values in previous studies used for pathogen deactivation (average irradiance of up to 2.73 $\mu W/cm^2$ at 1.7 m above the ground from Eadie et al.[42] and 3.5 $\mu W/cm^2$ from Peng et al.[23]). The range used in our model extends higher to take into account proposals for the use of significantly higher light fluence rates,[43] and include the fluence rates in our experiments (~45 $\mu W/cm^2$). Ventilation rates span a range of typical indoor values, and include the minimum American Society of Heating, Refrigerating and Air-Conditioning Engineers (ASHRAE) recommendations for homes (0.35 ACH), offices (~2-3 ACH), and health care settings (10 ACH).[44]

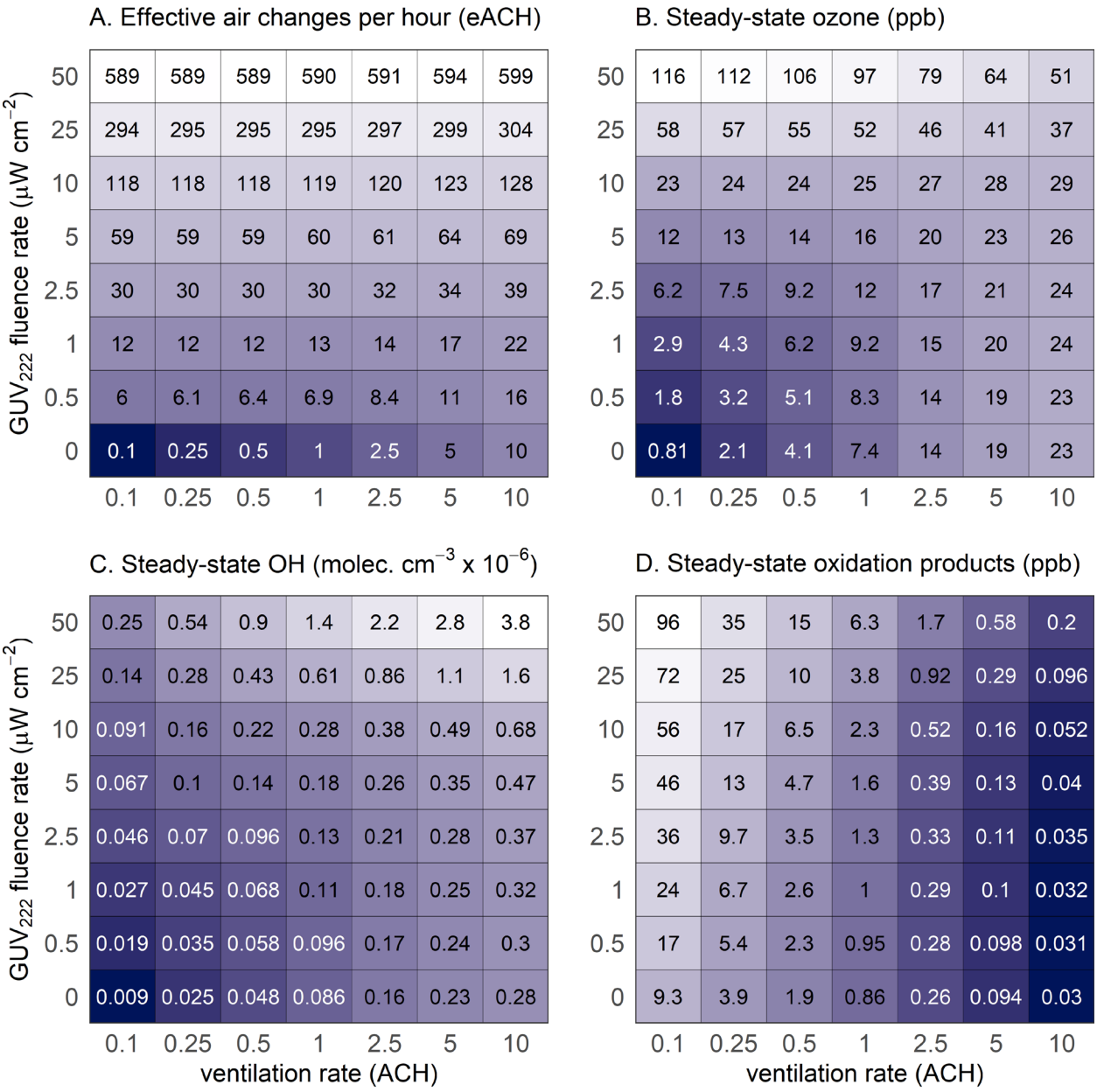

Figure 5: Effects of ventilation and GUV_{222} fluence rate on modeled GUV efficacy and indoor air quality (see also Figures S9-S12). Panel A: effective air changes per hour (eACH) for indoor pathogens, based on the previously reported inactivation rate of SARS-CoV-2 at 222 nm[45] (Section S4.2). Panels B-D: steady-state concentrations of (B) O_3, (C) OH, and (D) organic oxidation products, respectively, as predicted by the photochemical box model. Panel D calculations assume unit yields, and do not account for VOC production from surfaces (see Figure S11) or recycling by NO_x-HO_x interactions (Figure S12), so likely represent lower limits. Lighter colors represent larger values; note that the logarithmic color scaling is different for each panel. Additional model results are given in Figures S9 and S10.

Key model results are provided in Figure 5. Figure 5A shows the effective air change rate (eACH) across a wide range of GUV_{222} fluence and ventilation rates; even modest irradiation levels lead to substantial increases in eACH (see also Figure S9A). Figures 5B, C, and D show the steady-state indoor concentrations of O_3, OH, and total oxidation products (assuming unit yield), respectively.

Steady-state ozone levels (Figure 5B) are higher with 222 nm irradiation than without. Sources of O_3 include photochemistry (R1-2) and infiltration of outdoor air, while sinks include deposition, ventilation, and chemical reaction (rates and contributions of individual processes are given in Figures S9B-E). With low irradiation, O_3 levels are governed mainly by infiltration of outdoor air, and O_3 increases are modest. Under the highest fluence rates (>25 $\mu W/cm^2$), and especially under low ventilation rates (<1 ACH), indoor O_3 can reach levels exceeding that of the outdoors, and can even exceed the OSHA indoor limit of 100 ppb. However, even a small change in indoor O_3 levels can have a dramatic effect on people's total ozone exposure,[46] given the large fraction of time people spend indoors. In most cases, deposition represents the dominant sink of ozone (Figure S9D).

Figure 5C shows steady-state levels of OH as a function of ventilation and 222 nm light intensity. Sources of OH include O_3-alkene reactions (R3) and photochemistry (R4-5), while sinks are dominated by reactive losses (see also Figures S9F-G). In the absence of GUV_{222} irradiation, modeled OH is from alkene ozonolysis only, with predicted levels (~10^5 molec cm^{-3}) overlapping but falling on the low end of measured and modeled OH in indoor spaces (which range from $6x10^4$-$1.6x10^6$ molec cm^{-3});[47–56] this underestimate may arise from the omission of photolysis of trace species such as nitrous acid (HONO) or aldehydes, which may be important in some environments.[57] As with O_3, GUV_{222} irradiation leads to increases in indoor levels of OH. At low to moderate irradiation levels, this increase in OH is mostly due to the alkene ozonolysis reaction, while at higher levels, ozone photolysis plays a larger role (Figure S9G). OH increases with increasing photochemistry (higher GUV_{222} fluence rates and ozone concentrations), but is substantially modulated by losses from reaction with VOCs. VOC concentrations are higher at low ventilation rates (see Figure S9H), due to the buildup of emitted VOCs, which suppresses OH concentrations. At high light intensities, steady-state OH levels can approach outdoor levels, matching or exceeding indoor OH measurements during transient events such as cleaning or cooking activities.[58,59]

The production of O_3 and OH by GUV_{222}-driven chemistry and their subsequent reactions with VOCs leads to an increase in organic oxidation products (OVOCs and SOA). Steady-state levels and production rates of such products (assuming unit yields) are shown in Figures 5D and S9I. Concentrations increase with increased light intensity, and are especially high at low ventilation rates. Since more than one product molecule may be formed per oxidation reaction, and OVOCs may also be formed by surface reactions of O_3 or OH, these numbers likely represent lower limits. Of particular concern is the production of hazardous air pollutants (HAPs, such as CH_2O) and SOA, both of which may represent health hazards in the indoor environment. Concentrations of SOA are challenging to predict, as SOA production depends on the amounts and identity of the indoor VOCs, as well as on a host of reaction conditions. However, SOA levels on the order

of a few $\mu g/m^3$ might occur (Figure S10); the production of SOA from 222 nm irradiation in realistic indoor settings is an important area of future research.

The simplicity of the model neglects some additional secondary effects, which are highly uncertain. For example, volatile secondary organic products stemming from reactive surface losses of O_3 (e.g., to paint, textiles, skin)[12,60] could represent an additional secondary effect of GUV_{222} on indoor air quality. Preliminary modeling suggests that this may increase OVOC concentrations by as much as a factor of 100 (Figure S11). Similarly, indoor environments contain NO_X, which can affect the levels and fates of oxidants. While NO_X chemistry is not modeled explicitly here, due in part to uncertainties in NO_X photolysis processes, we have carried out additional simulations to estimate the role of HOx-NO_X cycling. As shown in Section S4.1 and Figure S12, such cycling increases OH concentrations and OVOC product formation substantially. We do not examine the role of HONO, which can be present in high (ppb) levels indoors[55] and absorbs strongly at 222 nm ($\sigma = 1.35 \times 10^{-18}$ cm^2 [9]); HONO photolysis may lead to even higher OH levels than predicted here. All of these effects have the potential to increase OVOC formation, suggesting that the OVOC concentrations presented in Figure 5 are best understood as a lower limit and that the indoor air quality impacts of 222 nm irradiation could be more severe than predicted here.

Implications

Our laboratory studies demonstrate that GUV_{222} light leads to the production of (1) ozone, (2) OH radicals, and (3) secondary organic species (OVOCs and SOA); these are in broad agreement with prior model predictions.[23] The resulting concentrations of such secondary species can be substantially higher than are normally found in indoor environments; in extreme cases, these increases can be dramatic, leading to oxidation conditions similar to those found in outdoor environments. The negative health impacts associated with the unavoidable generation of these secondary species – most importantly O_3, fine particular matter, and HAPs – thus need to be taken into account (and ideally mitigated) when considering the use of 222 nm disinfection in indoor spaces.

While a detailed analysis of the health impacts of GUV_{222} use (both the benefits from inactivation of airborne pathogens and the drawbacks from secondary pollutant formation) is beyond the scope of this work, our results offer some broad guidance as to the optimal use of GUV_{222} in indoor environments. Most importantly, GUV_{222} disinfection alone is not a safe substitute for ventilation as a means to control levels of indoor airborne pathogens, as it can lead to the buildup of indoor ozone and other pollutants to dangerous levels (Figure 5). However, GUV_{222} may be effectively used in conjunction with ventilation: relatively modest irradiation levels combined with carefully chosen ventilation conditions can greatly enhance the effective air change rate (Figure 5A), while limiting the levels of secondary pollutants (Figures 5B-D). Moreover, due to the unavoidable formation of secondary pollutants, GUV_{222} lights should be run at the lowest effective levels whenever possible. Further, the combination of GUV_{222} irradiation with air-cleaning technologies (e.g., sorbents for ozone and OVOCs, filters for particulate matter) may serve to minimize indoor secondary pollutant levels, potentially enabling

safer use of GUV_{222} under poorly-ventilated environments. Quantifying the benefits and tradeoffs of these combined approaches (ventilation, GUV_{222} irradiation, and/or air cleaning) in terms of pathogen transmission, air pollutant levels, human health, and cost-effectiveness, is a critical next step toward ensuring healthier indoor environments.

Supporting Information

Experimental conditions and methods, additional modeling methods, additional results and discussion (incl. ozone steady-state calculations, discussion of VOC loss pathways, discussion of elevated VOC and RH experiments, more complete product distribution figures, reaction schemes, and SMPS data), model results (incl. additional model output figures and calculation of effective air changes per hour) (PDF)

Acknowledgements and Funding Sources

This work is supported by the U.S. National Science Foundation under grants ECS-2108811 and AGS-2129835 and the Harvard Global Institute. The authors thank Bella Nesti (Harvard University) for assisting with the initial phases of data analysis, and Jose Jimenez (University of Colorado Boulder) for helpful discussions.

References

(1) Wells, W. F.; Wells, M. W.; Wilder, T. S. The Environmental Control of Epidemic Contagion: I. An Epidemiologic Study of Radiant Disinfection of Air in Day Schools. *American Journal of Epidemiology* **1942**, *35* (1), 97–121. https://doi.org/10.1093/oxfordjournals.aje.a118789.

(2) Nardell, E. A. Air Disinfection for Airborne Infection Control with a Focus on COVID-19: Why Germicidal UV Is Essential†. *Photochemistry and Photobiology* **2021**, *97* (3), 493–497. https://doi.org/10.1111/php.13421.

(3) Centers for Disease Control and Prevention. *Upper Room Ultraviolet Germicidal Irradiation (UVGI)*. https://www.cdc.gov/coronavirus/2019-ncov/community/ventilation/uvgi.html (accessed 2023-05-17).

(4) Blatchley, E. R.; Brenner, D.; Claus, H.; Cowan, T. E.; Linden, K.; Liu, Y.; Mao, T.; Park, S.-J.; Simons, R.; Sliney, D. *Far UV-C Radiation: Current State-of Knowledge*; White paper; International Ultraviolet Association Task Force.

(5) Buonanno, M.; Welch, D.; Shuryak, I.; Brenner, D. J. Far-UVC Light (222 Nm) Efficiently and Safely Inactivates Airborne Human Coronaviruses. *Sci Rep* **2020**, *10* (1), 10285. https://doi.org/10.1038/s41598-020-67211-2.

(6) Collins, D. B.; Farmer, D. K. Unintended Consequences of Air Cleaning Chemistry. *Environ. Sci. Technol.* **2021**, *55* (18), 12172–12179. https://doi.org/10.1021/acs.est.1c02582.

(7) Ye, Q.; Krechmer, J. E.; Shutter, J. D.; Barber, V. P.; Li, Y.; Helstrom, E.; Franco, L. J.; Cox, J. L.; Hrdina, A. I. H.; Goss, M. B.; Tahsini, N.; Canagaratna, M.; Keutsch, F. N.; Kroll, J. H. Real-Time Laboratory Measurements of VOC Emissions, Removal Rates, and Byproduct Formation from Consumer-Grade Oxidation-Based Air Cleaners. *Environ. Sci. Technol. Lett.* **2021**, *8* (12), 1020–1025. https://doi.org/10.1021/acs.estlett.1c00773.

(8) Turner, M. C.; Jerrett, M.; Pope, C. A.; Krewski, D.; Gapstur, S. M.; Diver, W. R.; Beckerman, B. S.; Marshall, J. D.; Su, J.; Crouse, D. L.; Burnett, R. T. Long-Term Ozone

Exposure and Mortality in a Large Prospective Study. *Am J Respir Crit Care Med* **2016**, *193* (10), 1134–1142. https://doi.org/10.1164/rccm.201508-1633OC.
(9) Burkholder, J.; Sander, S. P.; Abbatt, J. P. D.; Barker, J. R.; Cappa, C.; Crounse, J. D.; Dibble, T. S.; Huie, R. E.; Kolb, C. E.; Kurylo, M. J.; Orkin, V. L.; Percival, C. J.; Wilmouth, D. M.; Wine, P. H. *Chemical Kinetics and Photochemical Data for Use in Atmospheric Studies*; 19–5; NASA Jet Propulsion Laboratory, 2020.
(10) Nazaroff, W. W.; Weschler, C. J. Indoor Ozone: Concentrations and Influencing Factors. *Indoor Air* **2022**, *32* (1). https://doi.org/10.1111/ina.12942.
(11) Calvert, J. G. *The Mechanisms of Atmospheric Oxidation of the Alkenes*; Oxford University Press, 2000.
(12) Wisthaler, A.; Weschler, C. J. Reactions of Ozone with Human Skin Lipids: Sources of Carbonyls, Dicarbonyls, and Hydroxycarbonyls in Indoor Air. *Proceedings of the National Academy of Sciences* **2010**, *107* (15), 6568–6575. https://doi.org/10.1073/pnas.0904498106.
(13) Kroll, J. H.; Seinfeld, J. H. Chemistry of Secondary Organic Aerosol: Formation and Evolution of Low-Volatility Organics in the Atmosphere. *Atmospheric Environment* **2008**, *42* (16), 3593–3624. https://doi.org/10.1016/j.atmosenv.2008.01.003.
(14) US EPA. *Dose-Response Assessment for Assessing Health Risks Associated with Exposure to Hazardous Air Pollutants*. https://www.epa.gov/fera/dose-response-assessment-assessing-health-risks-associated-exposure-hazardous-air-pollutants (accessed 2023-05-02).
(15) Dockery, D. W.; Pope, C. A.; Xu, X.; Spengler, J. D.; Ware, J. H.; Fay, M. E.; Ferris, B. G.; Speizer, F. E. An Association between Air Pollution and Mortality in Six U.S. Cities. *New England Journal of Medicine* **1993**, *329* (24), 1753–1759. https://doi.org/10.1056/NEJM199312093292401.
(16) Burnett, R.; Chen, H.; Szyszkowicz, M.; Fann, N.; Hubbell, B.; Pope, C. A.; Apte, J. S.; Brauer, M.; Cohen, A.; Weichenthal, S.; Coggins, J.; Di, Q.; Brunekreef, B.; Frostad, J.; Lim, S. S.; Kan, H.; Walker, K. D.; Thurston, G. D.; Hayes, R. B.; Lim, C. C.; Turner, M. C.; Jerrett, M.; Krewski, D.; Gapstur, S. M.; Diver, W. R.; Ostro, B.; Goldberg, D.; Crouse, D. L.; Martin, R. V.; Peters, P.; Pinault, L.; Tjepkema, M.; van Donkelaar, A.; Villeneuve, P. J.; Miller, A. B.; Yin, P.; Zhou, M.; Wang, L.; Janssen, N. A. H.; Marra, M.; Atkinson, R. W.; Tsang, H.; Quoc Thach, T.; Cannon, J. B.; Allen, R. T.; Hart, J. E.; Laden, F.; Cesaroni, G.; Forastiere, F.; Weinmayr, G.; Jaensch, A.; Nagel, G.; Concin, H.; Spadaro, J. V. Global Estimates of Mortality Associated with Long-Term Exposure to Outdoor Fine Particulate Matter. *Proceedings of the National Academy of Sciences* **2018**, *115* (38), 9592–9597. https://doi.org/10.1073/pnas.1803222115.
(17) Pye, H. O. T.; Ward-Caviness, C. K.; Murphy, B. N.; Appel, K. W.; Seltzer, K. M. Secondary Organic Aerosol Association with Cardiorespiratory Disease Mortality in the United States. *Nat Commun* **2021**, *12* (1), 7215. https://doi.org/10.1038/s41467-021-27484-1.
(18) Donahue, N. M.; Drozd, G. T.; Epstein, S. A.; Presto, A. A.; Kroll, J. H. Adventures in Ozoneland: Down the Rabbit-Hole. *Phys. Chem. Chem. Phys.* **2011**, *13* (23), 10848–10857. https://doi.org/10.1039/C0CP02564J.
(19) Levy, H. Normal Atmosphere: Large Radical and Formaldehyde Concentrations Predicted. *Science* **1971**, *173* (3992), 141–143. https://doi.org/10.1126/science.173.3992.141.
(20) Bender, E. Disinfecting the Air with Far-Ultraviolet Light. *Nature* **2022**, *610* (7933), S46–S47. https://doi.org/10.1038/d41586-022-03360-w.

(21) Link, M. F.; Shore, A.; Hamadani, B. H.; Poppendieck, D. Ozone Generation from a Germicidal Ultraviolet Lamp with Peak Emission at 222 Nm. *Environ. Sci. Technol. Lett.* **2023**, *10* (8), 675–679. https://doi.org/10.1021/acs.estlett.3c00318.
(22) Peng, Z.; Day, D. A.; Symonds, G. A.; Jenks, O. J.; Stark, H.; Handschy, A. V.; de Gouw, J. A.; Jimenez, J. L. Significant Production of Ozone from Germicidal UV Lights at 222 Nm. *Environ. Sci. Technol. Lett.* **2023**, *10* (8), 668–674. https://doi.org/10.1021/acs.estlett.3c00314.
(23) Peng, Z.; Miller, S. L.; Jimenez, J. L. Model Evaluation of Secondary Chemistry Due to Disinfection of Indoor Air with Germicidal Ultraviolet Lamps. *Environ. Sci. Technol. Lett.* **2023**, *10* (1), 6–13. https://doi.org/10.1021/acs.estlett.2c00599.
(24) Ushio, Inc. Care222 Technical Specification Sheet. https://www.ushio.com/files/specifications/care222-filtered-far-uv-c-excimer-lamp-module-technical-data-sheet.pdf (accessed 2023-05-03).
(25) Krechmer, J.; Lopez-Hilfiker, F.; Koss, A.; Hutterli, M.; Stoermer, C.; Deming, B.; Kimmel, J.; Warneke, C.; Holzinger, R.; Jayne, J.; Worsnop, D.; Fuhrer, K.; Gonin, M.; de Gouw, J. Evaluation of a New Reagent-Ion Source and Focusing Ion–Molecule Reactor for Use in Proton-Transfer-Reaction Mass Spectrometry. *Anal. Chem.* **2018**, *90* (20), 12011–12018. https://doi.org/10.1021/acs.analchem.8b02641.
(26) Zaytsev, A.; Breitenlechner, M.; Koss, A. R.; Lim, C. Y.; Rowe, J. C.; Kroll, J. H.; Keutsch, F. N. Using Collision-Induced Dissociation to Constrain Sensitivity of Ammonia Chemical Ionization Mass Spectrometry (NH4+ CIMS) to Oxygenated Volatile Organic Compounds. *Atmos. Meas. Tech.* **2019**, *12* (3), 1861–1870. https://doi.org/10.5194/amt-12-1861-2019.
(27) DeCarlo, P. F.; Kimmel, J. R.; Trimborn, A.; Northway, M. J.; Jayne, J. T.; Aiken, A. C.; Gonin, M.; Fuhrer, K.; Horvath, T.; Docherty, K. S.; Worsnop, D. R.; Jimenez, J. L. Field-Deployable, High-Resolution, Time-of-Flight Aerosol Mass Spectrometer. *Anal. Chem.* **2006**, *78* (24), 8281–8289. https://doi.org/10.1021/ac061249n.
(28) Stewart, D. J.; Almabrok, S. H.; Lockhart, J. P.; Mohamed, O. M.; Nutt, D. R.; Pfrang, C.; Marston, G. The Kinetics of the Gas-Phase Reactions of Selected Monoterpenes and Cyclo-Alkenes with Ozone and the NO3 Radical. *Atmospheric Environment* **2013**, *70*, 227–235. https://doi.org/10.1016/j.atmosenv.2013.01.036.
(29) Aschmann, S. M.; Arey, J.; Atkinson, R. Kinetics and Products of the Reactions of OH Radicals with Cyclohexene, 1-Methyl-1-Cyclohexene, *Cis* -Cyclooctene, and *Cis* -Cyclodecene. *J. Phys. Chem. A* **2012**, *116* (38), 9507–9515. https://doi.org/10.1021/jp307217m.
(30) D'Anna, B.; Andresen, Ø.; Gefen, Z.; J. Nielsen, C. Kinetic Study of OH and NO 3 Radical Reactions with 14 Aliphatic Aldehydes. *Physical Chemistry Chemical Physics* **2001**, *3* (15), 3057–3063. https://doi.org/10.1039/B103623H.
(31) Grøntoft, T.; Raychaudhuri, M. R. Compilation of Tables of Surface Deposition Velocities for O3, NO2 and SO2 to a Range of Indoor Surfaces. *Atmospheric Environment* **2004**, *38* (4), 533–544. https://doi.org/10.1016/j.atmosenv.2003.10.010.
(32) Saunders, S. M.; Jenkin, M. E.; Derwent, R. G.; Pilling, M. J. Protocol for the Development of the Master Chemical Mechanism, MCM v3 (Part A): Tropospheric Degradation of Non-Aromatic Volatile Organic Compounds. *Atmospheric Chemistry and Physics* **2003**, *3* (1), 161–180. https://doi.org/10.5194/acp-3-161-2003.

(33) Hansel, A.; Scholz, W.; Mentler, B.; Fischer, L.; Berndt, T. Detection of RO2 Radicals and Other Products from Cyclohexene Ozonolysis with NH4+ and Acetate Chemical Ionization Mass Spectrometry. *Atmospheric Environment* **2018**, *186*, 248–255. https://doi.org/10.1016/j.atmosenv.2018.04.023.
(34) Aschmann, S. M.; Tuazon, E. C.; Arey, J.; Atkinson, R. Products of the Gas-Phase Reaction of O3 with Cyclohexene. *J. Phys. Chem. A* **2003**, *107* (13), 2247–2255. https://doi.org/10.1021/jp022122e.
(35) Barua, S.; Iyer, S.; Kumar, A.; Seal, P.; Rissanen, M. An Aldehyde as a Rapid Source of Secondary Aerosol Precursors: Theoretical and Experimental Study of Hexanal Autoxidation. *EGUsphere* **2023**, 1–24. https://doi.org/10.5194/egusphere-2023-128.
(36) Singer, B. C.; Coleman, B. K.; Destaillats, H.; Hodgson, A. T.; Lunden, M. M.; Weschler, C. J.; Nazaroff, W. W. Indoor Secondary Pollutants from Cleaning Product and Air Freshener Use in the Presence of Ozone. *Atmospheric Environment* **2006**, *40* (35), 6696–6710. https://doi.org/10.1016/j.atmosenv.2006.06.005.
(37) Wainman, T.; Zhang, J.; Weschler, C. J.; Lioy, P. J. Ozone and Limonene in Indoor Air: A Source of Submicron Particle Exposure. *Environmental Health Perspectives* **2000**, *108* (12), 1139–1145. https://doi.org/10.1289/ehp.001081139.
(38) Price, D. J.; Day, D. A.; Pagonis, D.; Stark, H.; Algrim, L. B.; Handschy, A. V.; Liu, S.; Krechmer, J. E.; Miller, S. L.; Hunter, J. F.; de Gouw, J. A.; Ziemann, P. J.; Jimenez, J. L. Budgets of Organic Carbon Composition and Oxidation in Indoor Air. *Environ. Sci. Technol.* **2019**, *53* (22), 13053–13063. https://doi.org/10.1021/acs.est.9b04689.
(39) Mattila, J. M.; Arata, C.; Abeleira, A.; Zhou, Y.; Wang, C.; Katz, E. F.; Goldstein, A. H.; Abbatt, J. P. D.; DeCarlo, P. F.; Vance, M. E.; Farmer, D. K. Contrasting Chemical Complexity and the Reactive Organic Carbon Budget of Indoor and Outdoor Air. *Environ. Sci. Technol.* **2022**, *56* (1), 109–118. https://doi.org/10.1021/acs.est.1c03915.
(40) International Commission on Non-Ionizing Radiation Protection (ICNIRP). Guidelines on Limits of Exposure to Ultraviolet Radiation of Wavelengths between 180 Nm and 400 Nm (Incoherent Optical Radiation). *Health Phys* **2004**, *87* (2), 171–186. https://doi.org/10.1097/00004032-200408000-00006.
(41) American Conference of Governmental Industrial Hygienists. *2023 Threshold Limit Values (TLVs) and Biological Exposure Indices (BEIs)*; 2023.
(42) Eadie, E.; Hiwar, W.; Fletcher, L.; Tidswell, E.; O'Mahoney, P.; Buonanno, M.; Welch, D.; Adamson, C. S.; Brenner, D. J.; Noakes, C.; Wood, K. Far-UVC (222 Nm) Efficiently Inactivates an Airborne Pathogen in a Room-Sized Chamber. *Sci Rep* **2022**, *12* (1), 4373. https://doi.org/10.1038/s41598-022-08462-z.
(43) Esvelt, K. M. Delay, Detect, Defend: Preparing for a Future in Which Thousands Can Release New Pandemics. *The Geneva Centre for Security and Policy*. November 2022.
(44) ASHRAE/ANSI Standard 62.1-2022. Ventilation and Acceptable Indoor Air Quality, 2022.
(45) Ma, B.; Linden, Y. S.; Gundy, P. M.; Gerba, C. P.; Sobsey, M. D.; Linden, K. G. Inactivation of Coronaviruses and Phage Phi6 from Irradiation across UVC Wavelengths. *Environ. Sci. Technol. Lett.* **2021**, *8* (5), 425–430. https://doi.org/10.1021/acs.estlett.1c00178.
(46) Weschler, C. J. Ozone's Impact on Public Health: Contributions from Indoor Exposures to Ozone and Products of Ozone-Initiated Chemistry. *Environ Health Perspect* **2006**, *114* (10), 1489–1496. https://doi.org/10.1289/ehp.9256.

(47) Weschler, C. J.; Shields, H. C. Production of the Hydroxyl Radical in Indoor Air. *Environ. Sci. Technol.* **1996**, *30* (11), 3250–3258. https://doi.org/10.1021/es960032f.
(48) Weschler, C. J.; Shields, H. C. Measurements of the Hydroxyl Radical in a Manipulated but Realistic Indoor Environment. *Environ. Sci. Technol.* **1997**, *31* (12), 3719–3722. https://doi.org/10.1021/es970669e.
(49) Carslaw, N. A New Detailed Chemical Model for Indoor Air Pollution. *Atmospheric Environment* **2007**, *41* (6), 1164–1179. https://doi.org/10.1016/j.atmosenv.2006.09.038.
(50) Waring, M. S.; Wells, J. R. Volatile Organic Compound Conversion by Ozone, Hydroxyl Radicals, and Nitrate Radicals in Residential Indoor Air: Magnitudes and Impacts of Oxidant Sources. *Atmospheric Environment* **2015**, *106*, 382–391. https://doi.org/10.1016/j.atmosenv.2014.06.062.
(51) Carslaw, N.; Fletcher, L.; Heard, D.; Ingham, T.; Walker, H. Significant OH Production under Surface Cleaning and Air Cleaning Conditions: Impact on Indoor Air Quality. *Indoor Air* **2017**, *27* (6), 1091–1100. https://doi.org/10.1111/ina.12394.
(52) Gligorovski, S.; Weschler, C. J. The Oxidative Capacity of Indoor Atmospheres. *Environ. Sci. Technol.* **2013**, *47* (24), 13905–13906. https://doi.org/10.1021/es404928t.
(53) Fiorentino, E.-A.; Chen, H.; Gandolfo, A.; Lannuque, V.; Sartelet, K.; Wortham, H. Measurements and Modelling of OH and Peroxy Radicals in an Indoor Environment Under Different Light Conditions and VOC Levels. *Atmospheric Environment* **2023**, *292*, 119398. https://doi.org/10.1016/j.atmosenv.2022.119398.
(54) Mendez, M.; Amedro, D.; Blond, N.; Hauglustaine, D. A.; Blondeau, P.; Afif, C.; Fittschen, C.; Schoemaecker, C. Identification of the Major HOx Radical Pathways in an Indoor Air Environment. *Indoor Air* **2017**, *27* (2), 434–442. https://doi.org/10.1111/ina.12316.
(55) Gómez Alvarez, E.; Amedro, D.; Afif, C.; Gligorovski, S.; Schoemaecker, C.; Fittschen, C.; Doussin, J.-F.; Wortham, H. Unexpectedly High Indoor Hydroxyl Radical Concentrations Associated with Nitrous Acid. *Proceedings of the National Academy of Sciences* **2013**, *110* (33), 13294–13299. https://doi.org/10.1073/pnas.1308310110.
(56) Zannoni, N.; Lakey, P. S. J.; Won, Y.; Shiraiwa, M.; Rim, D.; Weschler, C. J.; Wang, N.; Ernle, L.; Li, M.; Bekö, G.; Wargocki, P.; Williams, J. The Human Oxidation Field. *Science* **2022**, *377* (6610), 1071–1077. https://doi.org/10.1126/science.abn0340.
(57) Kowal, S. F.; Allen, S. R.; Kahan, T. F. Wavelength-Resolved Photon Fluxes of Indoor Light Sources: Implications for HOx Production. *Environ. Sci. Technol.* **2017**, *51* (18), 10423–10430. https://doi.org/10.1021/acs.est.7b02015.
(58) Rosales, C. M. F.; Jiang, J.; Lahib, A.; Bottorff, B. P.; Reidy, E. K.; Kumar, V.; Tasoglou, A.; Huber, H.; Dusanter, S.; Tomas, A.; Boor, B. E.; Stevens, P. S. Chemistry and Human Exposure Implications of Secondary Organic Aerosol Production from Indoor Terpene Ozonolysis. *Science Advances* **2022**, *8* (8), eabj9156. https://doi.org/10.1126/sciadv.abj9156.
(59) Reidy, E.; Bottorff, B. P.; Rosales, C. M. F.; Cardoso-Saldaña, F. J.; Arata, C.; Zhou, S.; Wang, C.; Abeleira, A.; Hildebrandt Ruiz, L.; Goldstein, A. H.; Novoselac, A.; Kahan, T. F.; Abbatt, J. P. D.; Vance, M. E.; Farmer, D. K.; Stevens, P. S. Measurements of Hydroxyl Radical Concentrations during Indoor Cooking Events: Evidence of an Unmeasured Photolytic Source of Radicals. *Environ. Sci. Technol.* **2023**, *57* (2), 896–908. https://doi.org/10.1021/acs.est.2c05756.

(60) Wang, H.; Morrison, G. Ozone-Surface Reactions in Five Homes: Surface Reaction Probabilities, Aldehyde Yields, and Trends. *Indoor Air* **2010**, *20* (3), 224–234. https://doi.org/10.1111/j.1600-0668.2010.00648.x.